JGR Space Physics

RESEARCH ARTICLE
10.1029/2021JA029468

Statistics on Omega Band Properties and Related Geomagnetic Variations

M. Vokhmyanin[1,2], S. Apatenkov[1], E. Gordeev[1], V. Andreeva[1], N. Partamies[3], K. Kauristie[4], and L. Juusola[4]

[1]Department of Earth's Physics, St. Petersburg State University, St. Petersburg, Russia, [2]Space Climate Research Group, Space Physics and Astronomy Research Unit, University of Oulu, Oulu, Finland, [3]Department of Geophysics, University Centre in Svalbard, Longyearbyen, Norway, [4]Finnish Meteorological Institute, Helsinki, Finland

Key Points:

- Superposed-epoch analysis confirmed the typical ground magnetic variations for omega structure—bipolar pulse in B_Y and short B_Z decrease
- Omega structures produce 50%–100% higher than averaged *dB/dt* during low and moderate geomagnetic activity
- Statistically confirmed that ground *dB/dt* value depends on omegas velocity and size

Correspondence to:
E. Gordeev,
evgeny.i.gordeev@spbu.ru

Citation:
Vokhmyanin, M., Apatenkov, S., Gordeev, E., Andreeva, V., Partamies, N., Kauristie, K., & Juusola, L. (2021). Statistics on omega band properties and related geomagnetic variations. *Journal of Geophysical Research: Space Physics*, *126*, e2021JA029468. https://doi.org/10.1029/2021JA029468

Received 21 APR 2021
Accepted 27 JUN 2021

Abstract Using the list of the omega structures based on the Magnetometers-Ionospheric Radars-All-sky Cameras Large Experiment network (Partamies et al., 2017, https://doi.org/10.5194/angeo-35-1069-2017), we obtained a number of important statistical characteristics describing the surface magnetic field. Based on 438 events, typical magnetic variations associated with the passage of the single omega were obtained. The typical variation, obtained using superposed epoch analysis, is associated with a local bending of the westward electrojet and statistically confirms the distribution of equivalent ionospheric currents obtained in earlier observations of single omegas. It was found that during low and moderate geomagnetic activity, the appearance of the omega structures in the dark morning magnetic local time (MLT) sector results in two times higher than average *dB/dt* on the ground surface. Also, the velocity, direction of movement, and area of omega structures were calculated. It is shown that faster and bigger omegas produce larger time derivatives of the ground magnetic field. Furthermore, we demonstrate that in the 03–08 MLT sector, superposed magnetic variations for the arbitrary events of very high time derivatives $|dB/dt| > 10$ nT/s, reveal magnetic signatures similar to omegas. Our findings, together with the results described by Apatenkov et al. (2020, https://doi.org/10.1029/2019gl086677), emphasize the important role of omega structures in the formation of large geomagnetically induced currents.

1. Introduction

Auroral omega bands are specific auroral forms emerging as a set of quasi-periodic long-living undulations in the poleward side of the diffuse aurora in the morning sector auroral oval, which have typical scale size from several hundred to several thousand kilometers, life time up to 100 min and drift eastward with the speed of 0.4–2 km/s (Akasofu & Kimball, 1964; Henderson et al., 2001; Sergeev et al., 2003). We should note that the term "omega" was originally referred to the dark area between two consecutive bright undulations of the diffuse aurora boundary (Akasofu, 1974; Akasofu & Kimball, 1964). However, the bright auroral object is easier to track than the dark one using all-sky camera (ASC). In recent years, the term "omega band" is often refers to the bright part of the classical omega band. Hereinafter, we use the term "omega" to describe the bright tongue since it can be often observed as a standalone unturned omega-shaped structure.

Based on the Magnetometers-Ionospheric Radars-All-sky Cameras Large Experiment (MIRACLE) ASC data from five identical Lapland stations, Partamies et al. (2017) have performed the largest statistical study of some omega band properties. Using semi-automated search methods, they detected 438 individual auroral omega structures in 1996–2007. Such representative statistics led to the following solid conclusions, complementing previous works. (a) Omega bands are typically observed in the morning sector toward the end of substorm expansion phase or during recovery phase (Akasofu, 1974; Opgenoorth et al., 1994). It is worth to note, the omega bands tend to appear during higher than average substorm activity, characterized by averaged local electrojet index IL = −250 nT, which is almost two times as intense as the average IL level for all substorms detected in this region (Partamies et al., 2015). (b) An average altitude of peak auroral emission within omega structures is 118 km. This gives an estimate of a few keV for the characteristic energy of precipitating electrons, which agrees with previous estimates (Amm et al., 2005; Wild et al., 2011). (c) Each individual omega was found to match with two-vortex equivalent Hall current structure associated with the pair of field-aligned currents where upward current corresponds to the bright part of omega undulation (Amm et al., 2005; Weygand et al., 2015).

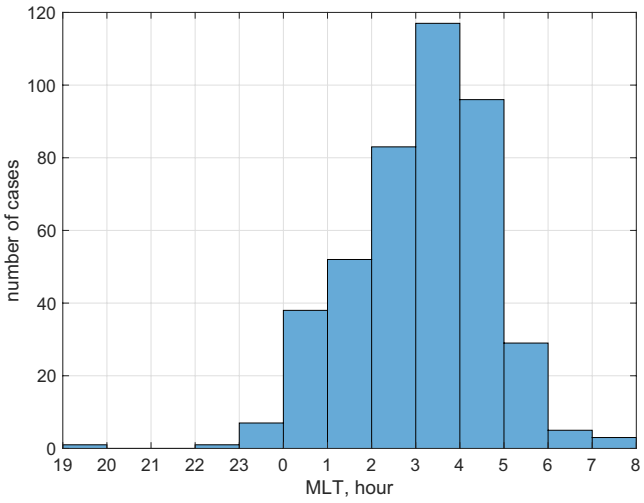

Figure 1. Magnetic local time distribution for the observed omega structures.

The same set of omega structures from Partamies et al. (2017) was used by Andreeva et al. (2021) to statistically investigate the omegas' source location. The authors projected the omegas from the ionosphere to the magnetospheric equatorial plane, using the recent empirical magnetic field model (Tsyganenko & Andreeva, 2016). Ionosphere-to-magnetosphere projection shows that the omegas' source is located relatively close to Earth at radial distances of 6–14 R_E, supporting previous case study results (Liu et al., 2018; Weygand et al., 2015; Wild et al., 2011). Velocity estimates for omega projections revealed the radial earthward propagation of the omegas' source region at a typical speed of several tens of km/s, in addition to expected eastward propagation observed in the ionosphere (Opgenoorth et al., 1983; Sergeev et al., 2003).

In the present study, we will further extend the set of characteristic omega properties using the same list of omegas from Partamies et al. (2017). Here, we will focus on the ground magnetic field perturbations, particularly *dB/dt* amplitudes, and their link to the kinematic characteristics such as size and drift velocity of omegas. The ground magnetic perturbations are of special interest for space weather applications since they cause geomagnetically induced currents (GICs) in long conducting systems—power grids, pipelines, and railway grids (Belakhovsky et al., 2019; Pirjola et al., 2005; Pulkkinen et al., 2017).

Inductive coupling between *dB/dt* and electric field that drives GIC is not linear due to the finite Earth's conductivity, so a large but short *dB/dt* impulse does not necessarily produce large GIC (Cagniard, 1953; Oyedokun et al., 2020). This nonlinearity in the *dB/dt*-GIC relationship is less pronounced for the lower frequency magnetic field variations with periods more than 1 min, including Pi3/Ps6 range of pulsations (Heyns et al., 2021) inherent to omega bands (Gustafsson et al., 1981; Jorgensen et al., 1999; Opgenoorth et al., 1983; Saito, 1978; Viljanen et al., 2001). This gives the confidence to use *dB/dt* as a proxy for GIC in the case of omega bands. In addition, it was shown in Apatenkov et al. (2020) that the largest GIC (>100 A) ever recorded in the Kola Peninsula power grid was caused by omega band activity, and the main inductive effect was linked to the spatial derivative associated with omega motion. Omega bands, being compact transient auroral phenomena, have localized but significant effects on the ground systems in high latitudes. In this study, we study this effect for the first time on a statistical basis.

This study is structured as follows. The ASC data and the ground magnetic field data for the utilized set of omega cases are described in the next section. Superposed ground magnetic variations are discussed in Section 3. In Section 4, we evaluate how the presence of omegas affects time derivatives of the geomagnetic field observed on the ground. In Section 5, we present the procedure to derive velocity, direction, and areas of the studied omega structures. In Section 6, we estimate the relation between maximum |*dB/dt*| and omega's velocity and area. Finally, in the discussion, we look at the typical magnetic variations corresponding to the extreme |*dB/dt*| > 10 nT/s cases.

2. Instruments and Data

Partamies et al. (2017) (hereinafter P17) provided a list of omega shape auroras that were observed with the ASCs at five MIRACLE network stations during 1996–2007. These stations are located in Fennoscandian Lapland at the auroral latitudes: Sodankylä (SOD, 63.92°N corrected geomagnetic latitude), Muonio (MUO, 64.72°N), Abisko (ABK, 65.30°N), Kilpisjärvi (KIL, 65.88°N), and Kevo (KEV, 66.32°N). P17 introduced a semi-automatic method to detect the omega shape auroras during the nighttime hours from September to April (when the Sun is more than 10° below the horizon). In our statistical study, we utilize the entire list of 438 omegas introduced in P17 paper.

Figure 1 shows the distribution of omegas' magnetic local time (MLT) when most of the structure was well observed within the camera field of view. The selected cases occupy 23–08 MLT with 68% of the omegas observed within 02–05 MLT morning sector. The majority of the events (335) corresponds to an individual

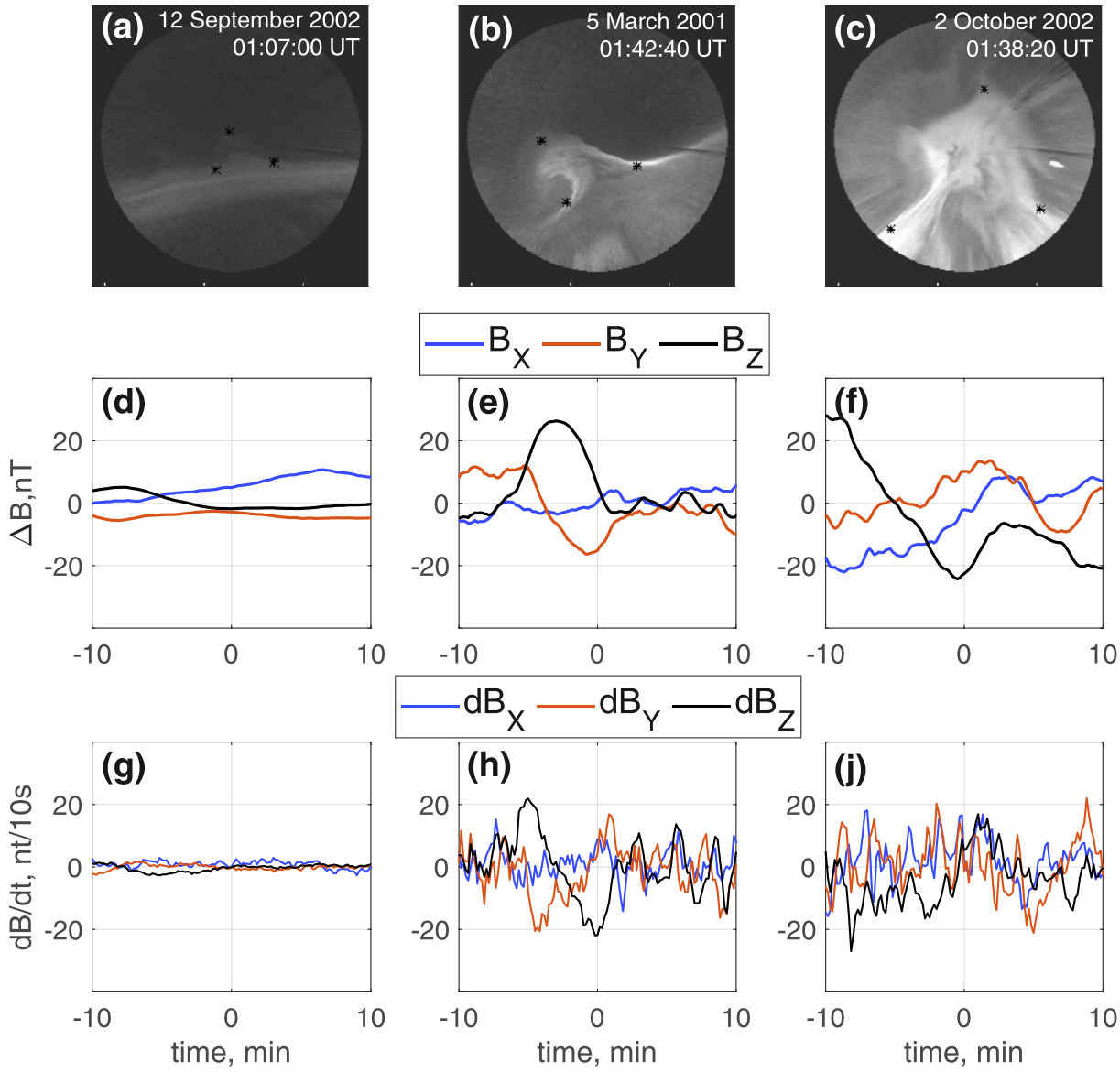

Figure 2. Examples of observed omega structures at Sodankylä. (a–c) the all-sky cameras images taken at 01:07:00 UT on September 12, 2002, 01:42:40 UT on 5 March 2001, and 01:38:20 UT on October 2, 2002. (d–j) The corresponding variations and time derivatives in *X* (blue), *Y* (red), and *Z* (black) components of the geomagnetic field (±10 min of the time when the images were taken).

omega, that is, the next omega appears after more than half an hour. The omegas are tracked within the ASC field of view from 4 to 15 min. Considering the average altitude of the observed in P17 omegas $h = 118$ km, the size of the omegas is restricted to the area of a circle with a diameter of about 600 km. Note that the horizontal scale size of omegas can be more than 1,000 km (Tanaka et al., 2015).

Ground magnetic data were provided by the IMAGE network magnetometers (Tanskanen, 2009) at 10 s time resolution at the same observatories with ASCs (20 s resolution). The time derivatives and the variations of the geomagnetic field are investigated in three field components: horizontal *X* (northward), horizontal *Y* (eastward), and vertical *Z* (directed to the Earth's center).

In Figure 2, we include three examples of the ASC images captured at Sodankylä station at the following times 01:07:00 UT on September 12, 2002, 01:42:40 UT on March 5, 2001, and 01:38:20 UT on October 2, 2002. These examples show a large diversity of the shape, size, and brightness of omega structures. Below, we show the variations and time derivatives of the geomagnetic field components measured by Sodankylä

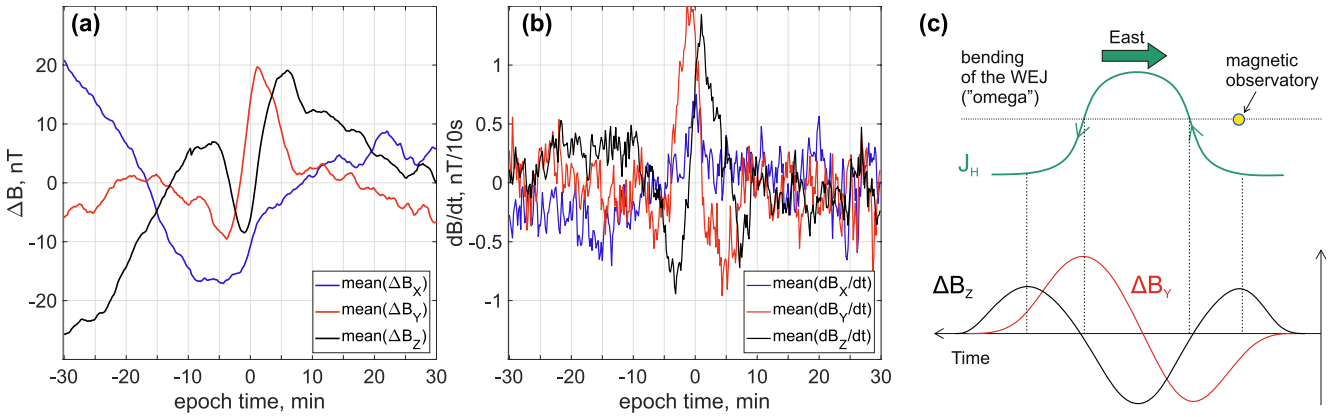

Figure 3. Superposed epoch analysis according to omega structure peak time (zero epoch time) for the: (a) Magnetic field and (b) Magnetic field time derivative. Blue, red, and black colors correspond to the *X*, *Y*, and *Z* components correspondingly. The sketch (c) Explains the observed magnetic variation: The bend of westward auroral electrojet propagates eastward (after Amm et al., 2005) and produces ground magnetic variation shown below (time goes to the left—opposite to the observations).

magnetometer within ±10 min around the noted time. The amplitude of the perturbations significantly increases for brighter and bigger structures in Figures 2b and 2c. On the contrary, no pronounced magnetic effects are seen near the peak time corresponding to the faint omega in Figure 2a.

Figure 2 shows that not every individual omega has specific and clear magnetic signatures. The variations are different in shape and amplitude. Thus, a superposed epoch method is used to study the typical magnetic variations associated with an omega passage.

3. Results

3.1. Superposed Geomagnetic Variations

Using the geomagnetic data of the IMAGE network, we select 1-h interval which was centered with respect to the peak time (Partamies et al., 2017), which is the time when the most omega-like structure was observed within the ASC field of view. The magnetic data were recorded during different years and seasons, so the baselines can differ dramatically. The averaged values were subtracted to be able to superpose and compare the magnetic variations. This is applied to every component. This is a very rough estimate of the background/baseline field. Nevertheless, this simple and fast procedure is suitable when studying the magnetic field variations rather than absolute values. Ps6 pulsations associated with omega bands (Saito, 1978) have periods 3–5 times shorter than 1 h, so the average value is expected to be close to the pulsations' "zero level."

Figure 3a shows superposed variations of *X* (geographic North), *Y* (geographic East), and *Z* (downwards) geomagnetic field components for the entire set of 438 observed omegas. We found a surprising fact that different individual magnetic recordings being summed up to show the distinct variation attributed to the omega passage. Two time scales can be distinguished within these magnetic signatures: (a) short—10 min around the omega, ±5 min close to zero epoch time, and (b) long—about 30 min preceding to the omega.

The short time scale can be explained by eastward propagation of the ionospheric current structure typical for the omega. Opgenoorth et al. (1983) and Amm et al. (2005) show the intense current directed equatorward at the western part of the omega carried mainly by Hall current. Clear bipolar variations in *Y* and *Z* field components can be explained by the eastward propagation of this equatorward (southward for IMAGE) current. At the −5 min time moment (Figure 3a), the current is on the west side from the station, at the +5 min time moment, the current propagates eastward and appears on the right side. We show this propagation schematically in Figure 3c. Note that time goes to the left on the sketch, that is, opposite to that in the observations.

The longer variation has no such straightforward and expected explanation, we interpret it as an equatorward expansion of the westward electrojet (WEJ). Decrease in B_X is caused by the approaching westward

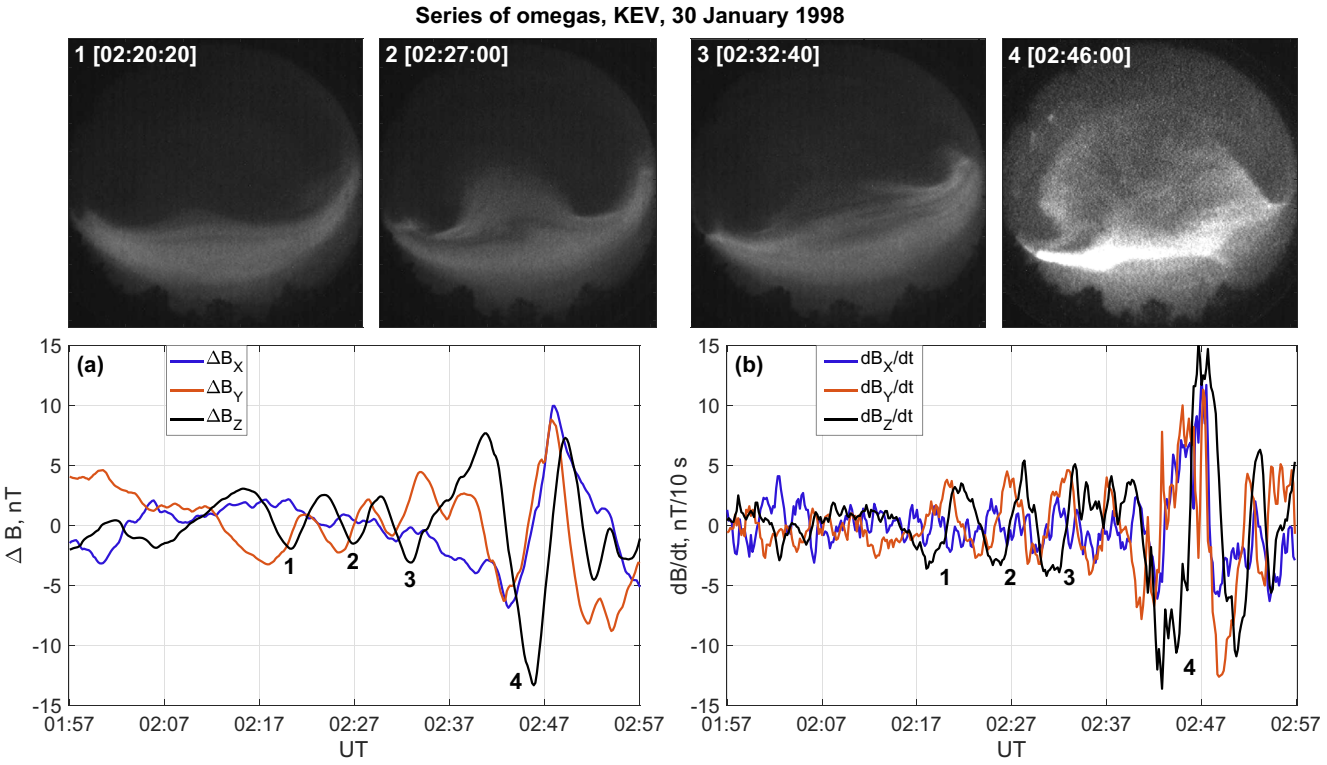

Figure 4. (a) Variations in the northward *X* (blue), eastward *Y* (red), and downward *Z* (black) geomagnetic field components at the Kevo station from 02 to 03 UT, January 30, 1998. The numbers in ASC images (doubled brightness) at the upper left corner correspond to the variations indicated with numbers 1–4; omega #2 is from the list by Partamies et al. (2017). (b) Time derivatives of the magnetic field components.

current and/or its intensity growth. The growth of B_Z and its sign change from negative to positive denotes the equatorward propagating WEJ: at −30 min time moment, the current was poleward from the station, at −10 min, the current was located overhead or even passed further equatorward. Note that the effect in Figure 3a is only a qualitative estimate. The amplitude of the effect is about 30 nT but might be significantly higher (see, e.g., Figure 4) for individual cases—the standard deviation of the field values observed within the ±5 min time is about 50–60 nT.

In Figure 3b, the average time derivatives (*dB/dt* is expressed in nT per 10 s) reveal the presence of the omega effect even more clearly. Distinctive *dB/dt* signature stands out from the background noise within the ±5 min of zero epoch time. Result in Figure 3b was obtained without any manipulations with the data, like background field subtraction, and should be considered as a more reliable evidence of the magnetic effect of the omegas. The mean amplitude of superposed time derivatives is about 1.0–1.5 nT/10 s, while the standard deviation of the observed values is about 4 nT/10 s. The most probable time to see the highest *dB/dt* is when the omega moves right over the observation site within ±5 min of zero epoch time. Overall, omegas increase the probability of high *dB/dt* observation, which is discussed in more detail in the next section.

An example of magnetic field variations at Kevo station on January 30, 1998 is shown in Figure 4. This example from the analyzed list nicely corresponds to the signature revealed in Figure 3a. For this event, the P17 list includes only one omega at 02:27 UT (omega #2 in Figure 4), while there are certainly more omega signatures within ±30 min interval. Four omega patterns are enumerated below the local minima of *Z* component (black curve). The ASC images shown on the top panel of Figure 4 confirm that each of these minima indeed corresponds to the auroral omega structure. During this event, the train of the observed omegas produces the quasi-periodic pulsations with 5–10 min period, resembling the known Ps6 type of pulsations observed in *Y* and *Z* components of the ground magnetic field in auroral zone and frequently accompanying omega bands (Gustafsson et al., 1981; Saito, 1978; Viljanen et al., 2001).

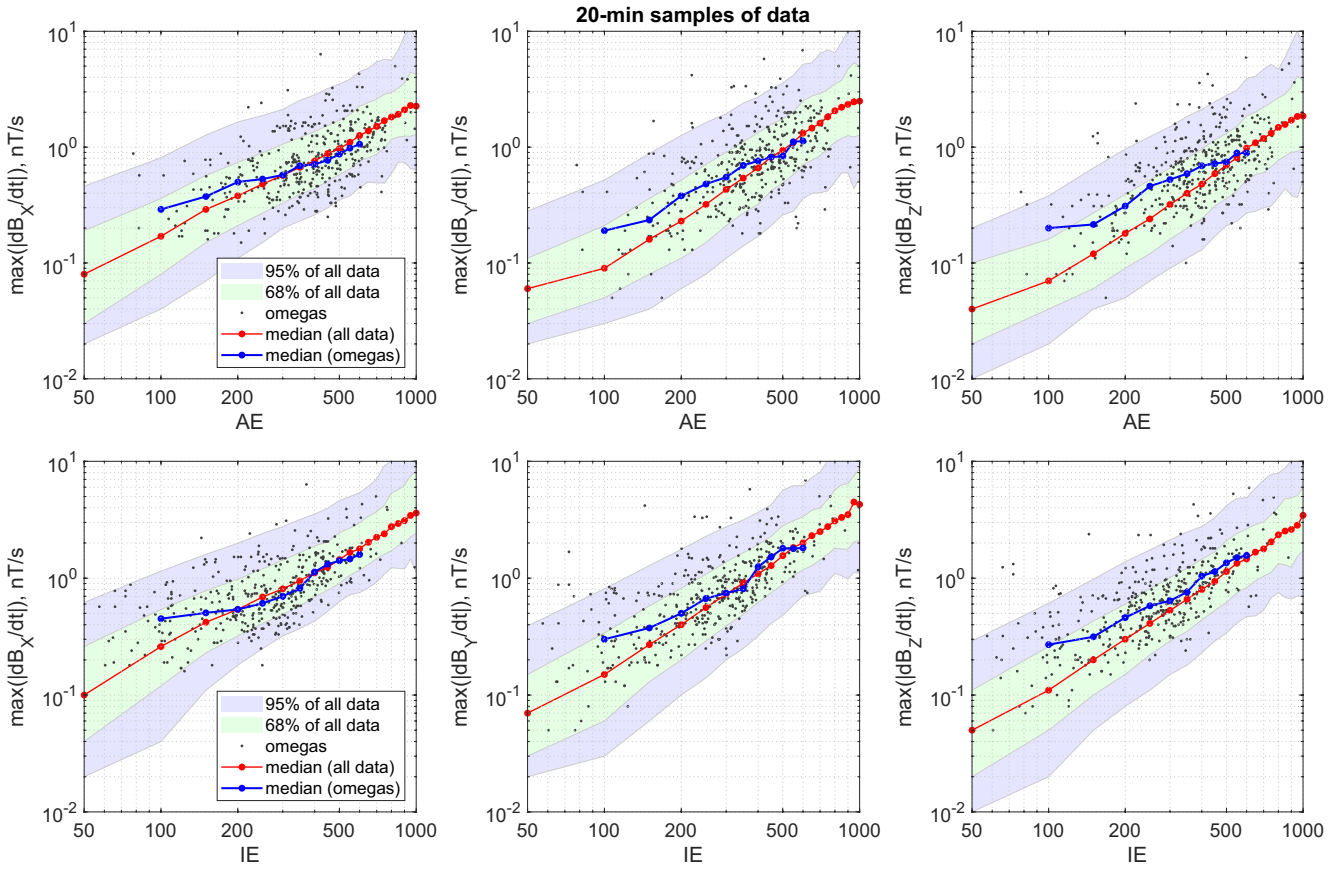

Figure 5. Comparing the time derivatives of the *X*, *Y*, and *Z* components of the geomagnetic field associated with omegas (scatterplot and blue curve) with all derivatives in this sector (shaded areas and red curve) with respect to the associated general AE and IE activity indices (in the upper and lower row respectively). Blue curve indicates median values for the omegas max|*dB/dt*| within the ±50 nT window of the corresponding activity index. Shaded areas characterize the distribution of maximum |*dB/dt*| values for all 20-min samples of the corresponding magnetic data depending on AE/IE indices. Red curve shows the median and shaded blue and green areas show 2.5%–97.5% and 16%–84% quantiles for all observed values of max|*dB/dt*| in this sector.

The amplitude of the magnetic effect from omegas 1, 2, and 3 is about 50 nT for both B_X and B_Y—two times the amplitude of the superposed epoch result. These three omegas occur within 20 min—about 7 min for each omega. Figure 4b shows that the corresponding time derivatives of B are about 5 nT/10 s. The biggest and brightest 4th omega causes the largest variations. Magnetic perturbation of about 150 nT corresponds to very high derivatives of about 10–15 nT/10 s in all magnetic components. The dependence of magnetic derivatives from the area covered by omega is investigated in Section 6.

3.2. Superposed Geomagnetic Variations

Omega structures may induce significant ground magnetic perturbations up to hundreds of nanoteslas. In the omega band event on June 29, 2013 studied by Apatenkov et al. (2020), time derivatives peaked at 15 nT/s (150 nT/10 s), which led to extremely high GIC in the power grid >100 A. The omega structures in that event were relatively big (120–150) × 10^3 km^2, as estimated from DMSP satellite UV images, and fast 0.5–1.7 km/s. Yet, it is interesting to estimate the derivatives of the ground magnetic field caused by more regular omegas from the P17 list.

In Figure 5, we show maximum |*dB/dt*| values (black dots) calculated from the 10 s magnetic observations within ±10 min of the average time when omega was seen at the ASC. The derivatives are placed against two geomagnetic indices (averaged within the analyzed 20 min samples) measuring the magnetic disturbance in the auroral zone: (a) global auroral electrojet AE index (Davis & Sugiura, 1966) which is calculated from the perturbations of H component at auroral observatories covering most of the longitude sectors, and

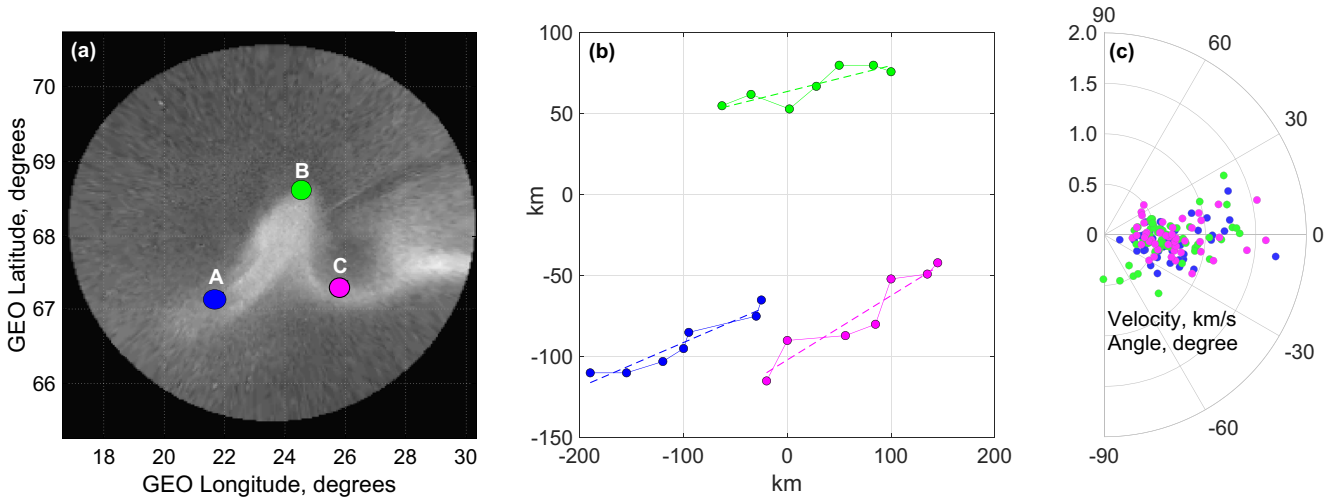

Figure 6. (a) Example of all-sky cameras image taken at Muonio on January 11, 2002 at 01:26 UT and three reference points for the analysis of omega velocity and area. (b) Linear fit of the coordinates of each point corresponding to consecutive images of this omega structure. (c) Polar plot for the angles and velocities obtained for the omegas observed at Muonio. Zero direction is the geomagnetic East.

(b) local IE electrojet indicator (Partamies et al., 2015) which is calculated in the same way but for IMAGE magnetometer network only. Blue curves indicate median values of maximum $|dB/dt|$ in the ±50 nT moving window. Clearly, higher $|dB/dt|$ in all three components of the geomagnetic field correspond to disturbed periods, that is, to higher AE and IE indices (note the logarithmic scale of both horizontal and vertical axes).

The effect of the omegas on the ground dB/dt can be estimated by comparing with the distribution of maximum $|dB/dt|$ values in arbitrary 20-min samples from IMAGE network selected for the similar conditions as observed for the omegas from the P17 list: the same time span (1997–2006) and MLT sector (01–05 MLT). In Figure 5, the distribution of maximum $|dB/dt|$ values in arbitrary 20-min samples are characterized by the median value, calculated in ±50 nT moving window (red curve), and four quantile levels, indicating 2.5%, 16%, 84% and 97.5% of all data within the window. Area between 2.5% and 97.5% is shaded blue. Area between 16% and 84% often related to ± one standard deviation for the normal distribution is shaded green.

Figure 5 reveals that for the same activity level, drifting omega structures produce larger changes in the ground magnetic field, specifically in the Y and Z components. Higher $|dB/dt|$ derivatives for omegas, as compared to baseline values obtained within 20-min samples, are more often observed during low and moderate geomagnetic activity below 250(200) nT for AE(IE) for B_X component, below 400(300) nT for B_Y component, and below 500(600) nT for B_Z component. Median values of the maximum $|dB/dt|$ for these ranges of AE and IE indices are on average 0.1–0.2 nT/s higher, which is 50%–100% higher than the baseline derivatives. Therefore, even regular omegas of small size (fit in the ASC field of view) on average lead to larger changes of the ground geomagnetic field.

3.3. Omega Motion

The drift of the omega structures can be investigated from the auroral observations. The ASC have 20-s cadence, so the majority of omegas from the P17 list were observed at several sequential frames during 1–15 min. To track the omega motion, we select three specific points connected to the omega shape, namely (A) western bottom, (B) top point, and (C) eastern bottom (Figure 6a). We admit this is subjective, however, the formal method has not been invented yet to our knowledge.

We also note the raw ASC images were mapped to the ionosphere assuming constant 118 km altitude. Near horizon pixels, 70°–90° from zenith, were removed as they bear large uncertainties. The mapping procedure described in Syrjäsuo (1996) transforms auroral ASC images into rectangular coordinates.

An example of point selection for omega tracking is shown in Figure 6a by blue, green, and purple circles corresponding to the previously described A, B, and C points. We assume the constant velocity for each

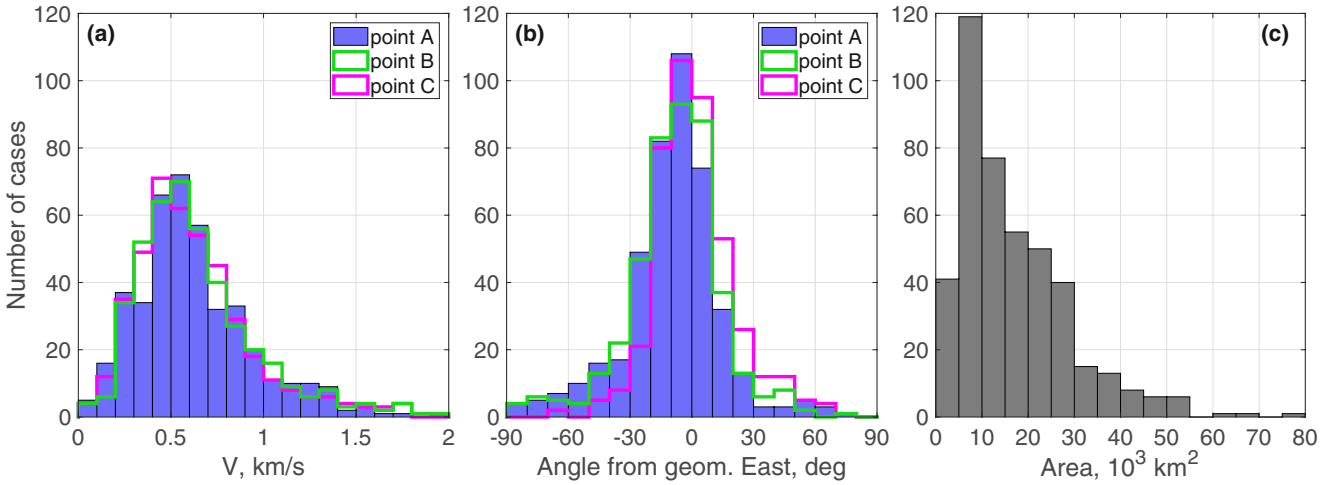

Figure 7. Distributions of omegas velocity (a), angle from geomagnetic East (b), and area (c).

point, allowing the velocities V_A, V_B, V_C to be different. The time sequence of point locations $X(t)$ is fitted by linear function. This is done independently for X, northward, and Y, eastward, coordinates. So, we find V_X and X_0 in the set of equations $X(t_i) = V_X t_i + X_0$. The same is done for V_Y and Y_0.

The fitting results are shown in Figure 6b. The dashed lines correspond to the coordinates obtained from the constant velocity approach. The velocities for points A, B, and C in this case slightly differ from each other. $V_A = (V_{AX}, V_{AY}) = (0.18, 0.68)$, $V_B = (0.10, 0.72)$, $V_C = (0.31, 0.73)$ km/s. To simplify reading and analysis, we further present velocity absolute value and its direction as the angle (in degrees) with respect to the geomagnetic East (positive is counterclockwise). The difference between geomagnetic and geographic East is about 11°. The (V_{AX}, V_{AY}) values from example above transform to ($|V|$, angle) values, giving $V_A = (0.70, 3.5)$, $V_B = (0.73, -3.5)$, $V_C = (0.79, 11.8)$.

In total, we managed to track 433 omega structures based on the P17 list (60 for ABK, 77 for KEV, 105 for KIL, 61 for MUO, and 130 for SOD). The resulting velocities and angles are summarized in Figure 6c for Muonio station and Figure 7 for all five sites. Figures 6c, 7a and 7b demonstrate that the speeds are in the 0.2–2 km/s range, the majority of the directions are within the −30° to +30° sector from the geomagnetic East, the main direction is definitely eastward. The most probable speed values are in the 0.2–0.8 km/s range, that is, in good agreement with previous case studies papers (e.g., Opgenoorth et al., 1983). We did not observe any significant difference between the distributions at any particular station; indeed, all ASCs are at a very narrow range of the magnetic latitudes.

There is a visual tendency that the omega velocity distribution is shifted slightly equatorward. The histograms of angle and speed distributions are presented in Figures 7a and 7b. The equatorward motion tendency is confirmed in Figure 7b, there are more omegas moving slightly equatorward (negative values of the angle) than poleward in addition to main eastward propagation. This equatorward drift can be related either to (a) earthward motion of the magnetospheric source or (b) to the overall expansion of the polar cap and the auroral oval during the substorm development. It is worth noting that if the first statement is correct, then this subtle north-south shift in the distribution of ionospheric velocities can lead to a significant radial velocity of the magnetospheric source. Indeed, in a recent study by Andreeva et al. (2021), the same set of omega cases was magnetically mapped to the equatorial magnetosphere. They showed that the magnetospheric counterpart statistically has the radial velocity component of several tens of km/s, which is comparable to the velocity in the azimuthal direction.

In addition to velocity, we provide rough estimation of the area covered by an omega shown in Figure 7c. We use triangles constructed from points A, B, and C (Figure 6a) to calculate this area. The average area during the omega passage is further considered. The area has values in the range (2–80) × 10^3 km^2 with the mean value 18 × 10^3 km^2. Note the upper limit for the omegas' area is instrumentally limited by the size of the ASC field of view in our study. The much larger omega structures have been observed by spaceborne imagers.

For example, using DMSP/SSUSI observations described by Apatenkov et al. (2020), we estimate the area of the omega structures associated with extreme GIC bursts as (120–150) $\times 10^3$ km^2. A similar area estimate for hypothetical auroral structures associated with the same GIC event was obtained by Chinkin et al. (2021).

3.4. Dependence on Omega Velocity and Area

To analyze how time derivatives of the ground magnetic field depend on omega velocity, we consider 433 cases with tracked omegas. As a very rough assumption, we can estimate the relation between ground magnetic field and velocity and area of omegas by considering a linear X-directed equivalent current J_X moving in Y direction above the station. This current may be roughly interpreted as a poleward-directed Hall current between two vortices of equivalent currents, associated with each individual omega. Time variation of the magnetic field B in a fixed point on the ground induced by a moving horizontal wire with current J_X (directed strictly northward) in the ionosphere is given by the expression following Biot-Savart law:

$$B(t) = \frac{\mu_0 J_X}{2\pi\sqrt{\left(H^2 + V^2 t^2\right)}}, \tag{1}$$

where H is the altitude of the equivalent currents (110 km), V is the velocity of the current moving in Y direction, t is the time from the omega peak (when the current is right above the station). In assumption of constant J_X and V, we obtain the time derivative for $B(t)$:

$$\frac{dB}{dt} = \frac{\mu_0 J_X V^2 t}{2\pi\sqrt{\left(H^2 + V^2 t^2\right)^3}}. \tag{2}$$

To get an expression for the maximum time derivative of the induced magnetic field, we find the root of the equation $(dB/dt)' = 0$ and substitute it to Equation 2:

$$\max\left(\frac{dB}{dt}\right) = \frac{\mu_0 J_X V}{3\pi\sqrt{3}H^2}. \tag{3}$$

Equation 3 indicates the linear dependence of maximum dB/dt on the omegas' velocity. Figure 8a, 8d, 8g and 8k show maximum values of time derivatives in 20 min intervals in X (a), Y (d), and Z (g) components of the geomagnetic field and its magnitude (k) versus the omegas' velocity (first column). Despite the large spread, the tendency for higher dB/dt occurrence during higher velocities is clearly seen, especially in the median values (red circles) for the corresponding ranges of V. Dependence is roughly linear, as predicted by Equation 3.

Here, we also investigate how dB/dt may depend on the area covered by the bright part of the omega (second column, Figure 8b, 8e, 8h and 8l). The logic behind it is that larger structures may be associated with stronger currents. Although this relation is weaker than for velocity, we still can see an increase in median dB/dt values. We also found that the relation is better between dB/dt and a product of velocity and area, where area is in the power of 1/3 (third column, Figure 8c, 8f, 8j and 8m). These figures indicate that faster and larger omegas provide higher time derivatives of the surface magnetic field.

4. Discussion

In the previous sections, we show that the currents flowing in auroral omega structures are associated with increased timed derivatives of the ground magnetic fields (Figure 5). The analyzed omegas are restricted in size by a 280 $\times 10^3$ km^2 circle area covered by the ASC field of view at 118 km altitude. For the P17 list, the largest area of a triangle formed by A, B, and C points is about 80 $\times 10^3$ km^2, one-third of the camera's field of view. Larger omegas cannot be tracked using ASCs. Besides, P17 list is a small fraction of the variety of omegas and lacks a representative set of extreme cases (big/fast/bright omegas). As we mentioned in Section 3.3, the extreme GIC case described in Apatenkov et al. (2020) had larger and brighter omega structures with up to 150 $\times 10^3$ km^2 areas and 2.5 km/s velocities.

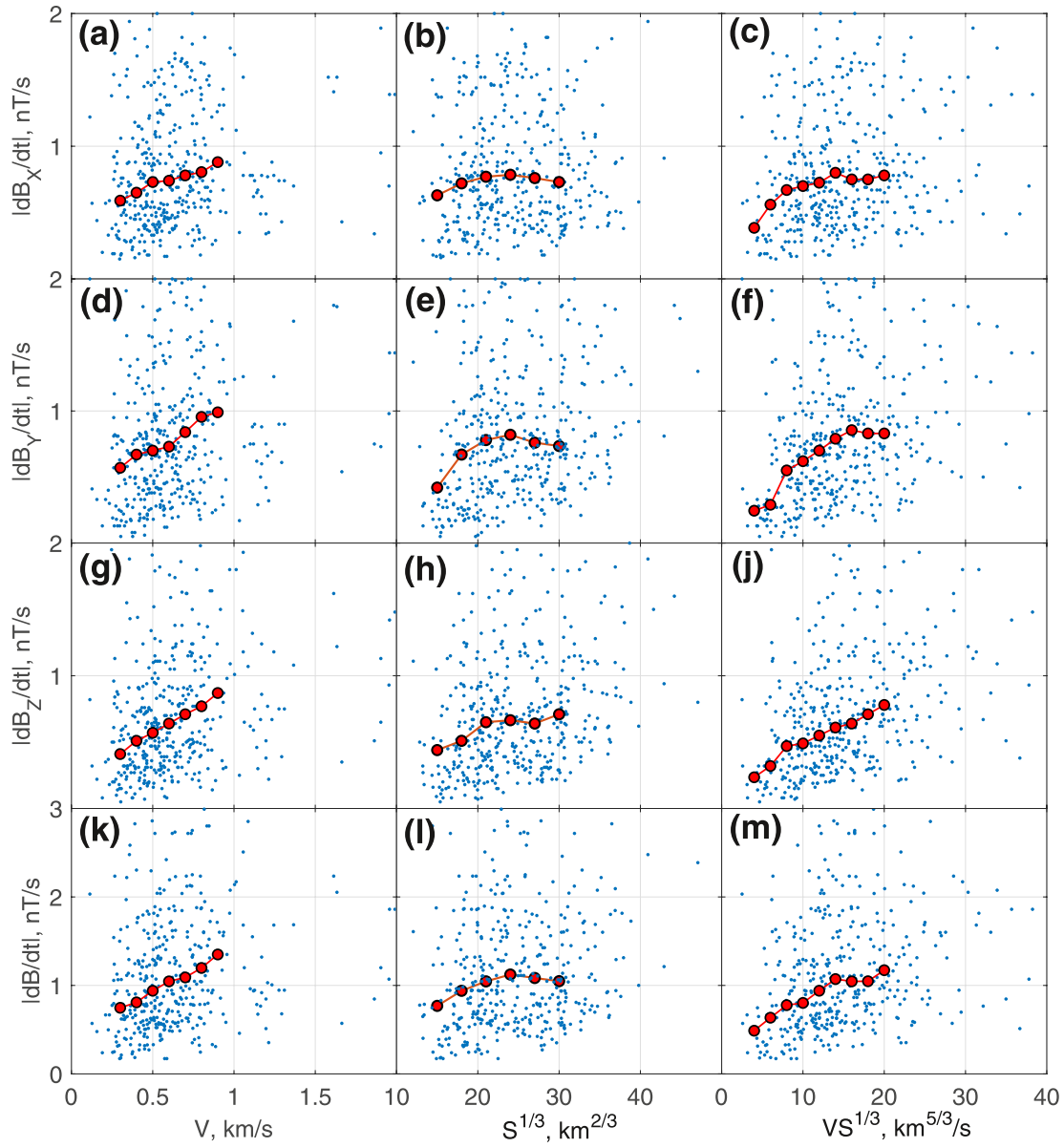

Figure 8. Maximum values of $|dB/dt|$ in X (a–c), Y (d–f), and Z (g–j) geomagnetic field components and their magnitudes (k–m) depending on the omegas' velocity (first column), area $S^{1/3}$ (second column) and $VS^{1/3}$ (third column). Red circles denote median values for the corresponding ranges of V, S, and $VS^{1/3}$.

Apatenkov et al. (2020) show that large-scale omega bands can be responsible for extremely high dB/dt values up to 15 nT/s. Using the same 10°s magnetic data of five stations during 1996–2018, we search for the time when $|dB/dt|$ was greater than 10 nT/s.

To find unique cases, we select only those that are separated by at least 1 h. This gives over 1,715 cases for five stations (1,046 in 00–12 MLT and 669 in 12–24 MLT). In Figure 9, the corresponding variations were superposed like in Section 3, with zero time being the time of maximum $|dB/dt|$. The results are shown separately for each hour within the 00–12 MLT sector. The interesting finding is that the omega-like magnetic signatures (Section 3, Figure 3a) are clearly observed in the 03–08 MLT sector: negative to positive B_Y change near zero epoch time and the same change in B_Z several minutes after.

Note that this MLT sector is characterized by the largest number of cases with $|dB/dt| > 10$ nT/s. This is similar to the Ps6 pulsation occurrence distribution (Rostoker & Barichello, 1980) with maximum in 04–06

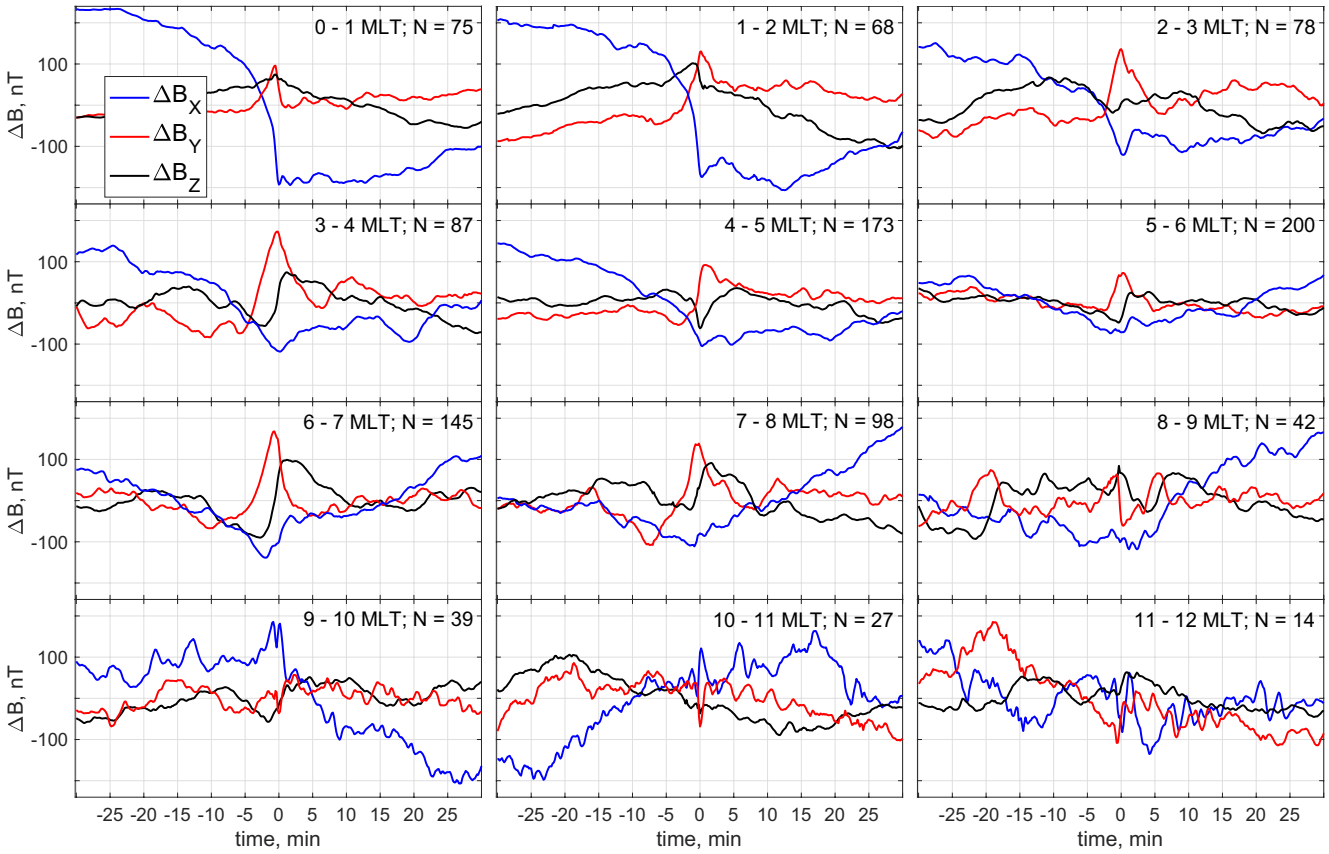

Figure 9. Superposed magnetic variations observed on five Fennoscandia stations with zero time being the time of maximum $|dB/dt| > 10$ nT/s. Number of cases and MLT sectors are shown in each panel.

MLT. Thus, we speculate that a significant part of the extreme ground *dB/dt* events at auroral latitudes might be associated with the passage of the omega bands, in agreement with Apatenkov et al. (2004).

5. Conclusions

In this study, we estimate the ground magnetic effect produced by the omega auroral structures. The list provided by Partamies et al., 2017 includes 438 omegas observed by the ASCs at the Fennoscandia region. The omegas from this list are highly versatile in form, size (limited by the ASC field of view), velocity, and brightness.

Typical magnetic signature of the ground magnetic perturbation due to omegas was estimated using superposed epoch analysis. We found that the typical magnetic variation has a short time signature: Depression of the *Z* and bipolar variation of the *Y* geomagnetic field components within ±5 min of the omega peak time (when the omega is above the site of the magnetic observations). This reflects the eastward propagation of the WEJ mesoscale bend which has almost north-south directed segments. The variations at the longer time scale, from 30 to 0 min before omega peak time, probably denote equatorward expansion of the WEJ which is seen in gradual decrease of *X* and increase of *Z* geomagnetic field components. This kind of WEJ behavior usually indicates the global convection growth or substorm expansion.

The moving current system associated with omega causes high *dB/dt* at the Earth's surface. We found that on average, the appearance of omega structures increases the rate of change in the surface magnetic field by 50%–100% for moderate geomagnetic activity level, as compared to all *dB/dt* in the morning sector.

We also track omega structures using three reference points manually selected on the ASC images and obtain their average velocities, directions and areas. The velocity range is 0.2–2 km/s with the average value of

0.7 km/s. The directions range from −30° to +30° from the geomagnetic East with the average value of −6° (to the South) indicating small equatorward motion.

Linear dependence was found between *dB/dt* and omega velocity, verifying that faster omegas induce higher *dB/dt* on the ground. Although the omega size seems to have a weaker effect on *dB/dt*, the product of the velocity and area shows better correlation than with only velocity.

Moreover, it was found that the highest *dB/dt* values observed at the Fennoscandia region in 1996–2018 within 03–08 MLT sector resemble the omega magnetic signatures. Extremely big/intense/fast omega structures therefore might be responsible for the fast changes of the ground magnetic field and thus triggering the formation of intense GIC.

Data Availability Statement

The MIRACLE data could be requested at https://space.fmi.fi/MIRACLE/. The list of omega events from Partamies et al. (2017) is available at http://doi.org/10.5281/zenodo.4541669.

Acknowledgments
The authors thank the institutes who maintain the IMAGE Magnetometer Array: Tromsø Geophysical Observatory of UiT, the Arctic University of Norway (Norway), Finnish Meteorological Institute (Finland), Institute of Geophysics Polish Academy of Sciences (Poland), GFZ German Research Centre for Geosciences (Germany), Geological Survey of Sweden (Sweden), Swedish Institute of Space Physics (Sweden), Sodankylä Geophysical Observatory of the University of Oulu (Finland), and Polar Geophysical Institute (Russia). The study by M. Vokhmyanin, V. Andreeva, S. Apatenkov, and E. Gordeev was supported by Russian Science Foundation grant 19-77-10016. The study of L. Juusola and K. Kauristie was supported by the Academy of Finland (decision 314670). The visits of V. Andreeva, S. Apatenkov, and E. Gordeev to FMI were supported by the Academy of Finland fund: Space Cooperation in the Science and Technology Commission between Finland and Russia (TT/AVA).

References

Akasofu, S. I. (1974). A study of auroral displays photographed from the DMSP-2 satellite and from the Alaska meridian chain of stations. *Space Science Reviews*, *16*, 617–725. https://doi.org/10.1007/BF00182598

Akasofu, S. I., & Kimball, D. S. (1964). The dynamics of the aurora-1: Instabilities of the aurora. *Journal of Atmospheric and Terrestrial Physics*, *26*, 205–211. https://doi.org/10.1016/0021-9169(64)90147-3

Amm, O., Aksnes, A., Stadsnes, J., Ostgaard, N., Vondrak, R. R., Germany, G. A., et al. (2005). Mesoscale ionospheric electrodynamics of omega bands determined from ground-based electromagnetic and satellite optical observations. *Annales Geophysicae*, *23*, 325–342. https://doi.org/10.5194/angeo-23-325-2005

Andreeva, V. A., Apatenkov, S. V., Gordeev, E. I., Partamies, N., & Kauristie, K. (2021). Omega band magnetospheric source location: A statistical model-based study. *Journal of Geophysical Research: Space Physics*, *126*, e2020JA028997. https://doi.org/10.1029/2020JA028997

Apatenkov, S. V., Pilipenko, V. A., Gordeev, E. I., Viljanen, A., Juusola, L., Belakhovsky, V. B., et al. (2020). Auroral omega bands are a significant cause of large geomagnetically induced currents. *Geophysical Research Letters*, *47*, e2019GL086677. https://doi.org/10.1029/2019GL086677

Apatenkov, S. V., Sergeev, V. A., Pirjola, R., & Viljanen, A. (2004). Evaluation of the geometry of ionospheric current systems related to rapid geomagnetic variations. *Annales Geophysicae*, *22*, 63–72. https://doi.org/10.5194/angeo-22-63-2004

Belakhovsky, V., Pilipenko, V., Engebretson, M., Sakharov, Y., & Selivanov, V. (2019). Impulsive disturbances of the geomagnetic field as a cause of induced currents of electric power lines. *Journal of Space Weather and Space Climate*, *9*, A18. https://doi.org/10.1051/swsc/2019015

Cagniard, L. (1953). Basic theory of the magneto-telluric method of geophysical prospecting. *Geophysics*, *18*, 605–635. https://doi.org/10.1190/1.1437915

Chinkin, V. E., Soloviev, A. A., Pilipenko, V. A., Engebretson, M. J., & Sakharov, Y. A. (2021). Determination of vortex current structure in the high-latitude ionosphere with associated GIC bursts from ground magnetic data. *Journal of Atmospheric and Solar-Terrestrial Physics*, *212*, 105514. https://doi.org/10.1016/j.jastp.2020.105514

Davis, T. N., & Sugiura, M. (1966). Auroral electrojet activity index AE and its universal time variations. *Journal of Geophysical Research*, *71*(3), 785–801. https://doi.org/10.1029/JZ071i003p00785

Gustafsson, G., Baumjohann, W., & Iversen, I. (1981). Multi-method observations and modelling of the three-dimensional currents associated with a very strong Ps6 event. *Journal of Geophysics*, *49*, 138–145.

Henderson, M. G., Kepko, L., Spence, H., Connors, M., Sigwarth, J., Frank, L., et al. (2001). The evolution of north-south aligned auroral forms into auroral torch structures: The generation of omega bands and ps6 pulsations via flow bursts. *Paper presented at the Sixth International Conference on Substorms* (pp. 169–174). Los Alamos National Laboratory.

Heyns, M. J., Lotz, S. I., & Gaunt, C. T. (2021). Geomagnetic pulsations driving geomagnetically induced currents. *Space Weather*, *19*, e2020SW002557. https://doi.org/10.1029/2020SW002557

Jorgensen, A. M., Spence, H. E., Hughes, T. J., & McDiarmid, D. (1999). A study of omega bands and Ps6 pulsations on the ground, at low altitude and at geostationary orbit. *Journal of Geophysical Research*, *104*(A7), 14705–14715. https://doi.org/10.1029/1998JA900100

Liu, J., Lyons, L. R., Archer, W. E., Gallardo-Lacourt, B., Nishimura, Y., Zou, Y., et al. (2018). Flow shears at the poleward boundary of omega bands observed during conjunctions of Swarm and THEMIS ASI. *Geophysical Research Letters*, *45*, 1218–1227. https://doi.org/10.1002/2017GL076485

Opgenoorth, H. J., Oksman, J., Kaila, K. U., Nielsen, E., & Baumjohann, W. (1983). Characteristics of eastward drifting omega bands in the morning sector of the auroral oval. *Journal of Geophysical Research*, *88*, 9171–9185. https://doi.org/10.1029/ja088ia11p09171

Opgenoorth, H. J., Persson, M. A. L., Pulkkinen, T. I., & Pellinen, R. J. (1994). Recovery phase of magnetospheric substorms and its association with morning sector aurora. *Journal of Geophysical Research*, *99*, 4115–4129. https://doi.org/10.1029/93JA01502

Oyedokun, M. H., Cilliers, P., Gaunt, C., & Gaunt, C. (2020). Frequency components of geomagnetically induced currents for power system modelling. *Paper presented at the 2020 International 490 SAUPEC/RobMech/PRASA Conference, Cape Town, South Africa, 2020* (pp. 1–6). IEEE. https://doi.org/10.1109/SAUPEC/RobMech/PRASA48453.2020.9041021

Partamies, N., Juusola, L., Whiter, D., & Kauristie, K. (2015). Substorm evolution of auroral structures. *Journal of Space Weather and Space Climate*, *120*, 5958–5972. https://doi.org/10.1002/2015JA021217

Partamies, N., Weygand, J. M., & Juusola, L. (2017). Statistical study of auroral omega bands. *Annales Geophysicae*, *35*, 1069–1083. https://doi.org/10.5194/angeo-35-1069-2017

Pirjola, R., Kauristie, K., Lappalainen, H., Viljanen, A., & Pulkkinen, A. (2005). Space weather risk. *Space Weather*, *3*, S02A02. https://doi.org/10.1029/2004SW000112

Pulkkinen, A., Bernabeu, E., Thomson, A., Viljanen, A., Pirjola, R., Boteler, D., et al. (2017). Geomagnetically induced currents: Science, engineering, and applications readiness. *Space Weather*, *15*, 828–856. https://doi.org/10.1002/2016SW001501

Rostoker, G., & Barichello, J. C. (1980). Seasonal and diurnal variation of Ps6 magnetic disturbances. *Journal of Geophysical Research*, *85*(A1), 161–163. https://doi.org/10.1029/JA085iA01p00161

Saito, T. (1978). Long-period irregular magnetic pulsation, Pi3. *Space Science Reviews*, *21*, 427–467. https://doi.org/10.1007/BF00173068

Sergeev, V. A., Yahnin, D. A., Liou, K., Thomsen, M. F., & Reeves, G. D. (2003). Narrow plasma streams as a candidate to populate the inner magnetosphere. In T. I. Pulkkinen, N. A. Tsyganenko, & R. H. W. Friedel (Eds.), *The inner magnetosphere, Geophysical Monograph Series* (pp. 55–60). American Geophysical Union. https://doi.org/10.1029/155GM07

Syrjäsuo, M. (1996). *All-sky camera (Master's Thesis)*. Helsinki University of Technology.

Tanaka, Y., Ogawa, Y., Kadokura, A., Partamies, N., Whiter, D., Enell, C.-F., et al. (2015). Eastward-expanding auroral surges observed in the post-midnight sector during a multiple-onset substorm. *Earth, Planet and Space*, *67*, 182. https://doi.org/10.1186/s40623-015-0350-8

Tanskanen, E. I. (2009). A comprehensive high-throughput analysis of substorms observed by IMAGE magnetometer network: Years 1993–2003 examined. *Journal of Geophysical Research*, *114*, A05204. https://doi.org/10.1029/2008JA013682

Tsyganenko, N. A., & Andreeva, V. A. (2016). An empirical RBF model of the magnetosphere parameterized by interplanetary and ground-based drivers. *Journal of Geophysical Research: Space Physics*, *121*(11), 10786–10802. https://doi.org/10.1002/2016JA023217

Viljanen, A., Nevanlinna, H., Pajunpää, K., & Pulkkinen, A. (2001). Time derivative of the horizontal geomagnetic field as an activity indicator. *Annales Geophysicae*, *19*(9), 1107–1118. https://doi.org/10.5194/angeo-19-1107-2001

Weygand, J. M., Kivelson, M. G., Frey, H. U., Rodriguez, J. V., Angelopoulos, V., Redmon, R., et al. (2015). An interpretation of spacecraft and ground based observations of multiple omega band events. *Journal of Atmospheric and Solar-Terrestrial Physics*, *133*, 185–204. https://doi.org/10.1016/j.jastp.2015.08.014

Wild, J. A., Woodfield, E. E., Donovan, E., Fear, R. C., Grocott, A., Lester, M., et al. (2011). Midnight sector observations of auroral omega bands. *Journal of Geophysical Research*, *116*, A00I30. https://doi.org/10.1029/2010JA015874